Tidal vorticity
Bottom topography
Current measurements
Southern North Sea
Spatial variability of currents

Vorticité de la marée
Topographie du fond
Courantométrie
Mer du Nord
Variabilité spatiale des courants

Topographically induced tidal vorticity in a shallow homogeneous sea area

H. W. RIEPMA
Royal Netherlands Meteorological Institute, P.O. Box 201, 3730 AE De Bilt, The Netherlands.

Received 5/1/87, in revised form 12/6/87, accepted 9/7/87.

ABSTRACT

In this paper we present some results of current measurements that were conducted in the southern bight of the North Sea. The object of these measurements was to study topographically induced tidal vorticity experimentally, as opposed to the theoretical studies of Zimmerman (1978; 1980).
Good agreement between theory and experiment was found only for the dominant semi-diurnal M_2 tidal component. Because of measurement errors, such an agreement could not be established for the M_4 tidal component.
The motivation for this study came from earlier observations of currents in the North Sea that revealed the existence of spatial variability of tidal and residual currents. Because vorticity is defined in terms of derivatives of the horizontal-flow components, it is a measure of spatial current variability as well.

Oceanol. Acta, 1987, **10**, 4, 393-401.

RÉSUMÉ

Vorticité de marée induite par la topographie dans une mer homogène peu profonde

Cet article présente quelques résultats de courantométrie obtenus dans la partie méridionale de la Mer du Nord. L'objectif des mesures était d'étudier expérimentalement la vorticité de marée induite par la topographie, en complément des travaux théoriques de Zimmermann (1978;1980).
Un bon accord a été trouvé entre la théorie et l'expérience uniquement pour la composante principale semi-diurne M2 de la marée. Les erreurs de mesure n'ont pas permis de retrouver cet accord pour la composante M4 de la marée.
La motivation de cette étude a pour origine des mesures antérieures des courants dans la Mer du Nord et l'observation de la variabilité spatiale des courants de marée et des courants résiduels. Comme la vorticité est définie par dérivation des composantes du flux horizontal, elle constitue une mesure de la variabilité spatiale du courant.

Oceanol. Acta, 1987, **10**, 4, 393-401.

INTRODUCTION

In recent years, several current-measuring campaigns showed that, within an apparent homogeneous sea area, spatial variability of tidal and residual currents may be manifest over relatively short distances (10 km). Herein, we define the residual current as an average over two M_2 tidal periods. However, this variability raises difficulties if the measurements are to be used for the description of the current system of a particular sea area. Riepma (1980), in his study of the in/out data set of Jonsdap 76, refers to this problem explicitly. Riepma (1985) reports on an experiment in the southern bight of the North Sea in which the trajectory of a rhodamine dye is considered while the dye patch floats through a dense currentmeter network to resolve small-scale spatial variability of currents.

For open shallow homogeneous sea areas, bottom topography seems to be the primary cause of variability, and several authors have studied this interaction problem. Some of these authors are concerned with vorticity arguments while others focus on the description of currents. Because our interest is in vorticity, the latter may be transformed by taking the curl of their results.

Yasuda (1980) considers the mechanism of horizontal friction in the coastal boundary layer if a no-slip condition is imposed. According to his estimates, the coastal boundary-layer thickness is approximately 1 km. Similar studies were reported by Tee (1977) and Yanagi (1976). Because of the distance from the coast, the coastal boundary-layer studies are not relevant to our experiments.

An interesting study, valid for the open sea, was presented by Huthnance (1973) for the tide-induced residual currents over the Norfolk sandbanks. Huthnance was able to show clockwise residual circulation around these banks. Other studies on rectified tidal currents were reported by Magnell *et al.* (1980) and Butman *et al.* (1983) near Georges Bank where also clockwise residual circulations were observed.

Although the above-mentioned studies revealed some evidence of the generation of residual current systems by the tidal current flowing over the bottom, it is by no means the only generating source for residual currents. Loder (1980) states that, over Georges Bank, thermohaline circulations may be of equal importance. Because our experiments are situated in a homogeneous sea area, we will not deal with these types of circulation.

On the other hand, Komen and Riepma (1981 *a*) show how wind induced currents may locally be guided by bottom topography. Because wind-induced currents have generally low frequencies, they are included in our definition of residual currents. Also, Riepma (1986) found strong experimental evidence that wind is the key to understanding residual vorticity generation.

It appears that the study of residual currents in some cases may not be relevant if the interest lies in the interaction of tidal currents with bottom topography, because there is a variety of generating sources that may not be separated clearly. As a matter of fact, Komen and Riepma (1981 *b*) indicate that wind-induced residual vorticity dominates for most of the time the tide-induced residual vorticity in the Southern Bight.

Because of the difficulties described above, it is logical to investigate experimentally the generation of tidal vorticity by topography supplementary to the generation of residual vorticity. The reason is that, in the frequency domain, the tidal-current components are relatively well defined compared to the residual currents which, as defined herein, cover a broad spectrum of low-frequency motions.

THEORY

This section will deal mainly with the theoretical aspects of our experiment. A discussion of the physical processes responsible for vorticity generation was given by Robinson (1981), and Zimmerman (1978; 1980) gave a mathematical treatment. For the convenience of the reader, a very short derivation of Zimmerman's results is given in this paper. For a full understanding, we refer to the original work.

The tidal-velocity field is assumed to be quasi-two dimensional. In that case, the relative vorticity ω is pointing vertically upward and is defined by

$$\omega = \frac{\partial v}{\partial x} - \frac{\partial u}{\partial y}, \tag{1}$$

where the x-axis is parallel to the major axis of the tidal ellipse and the y-axis is perpendicular to it. The depth-averaged velocity components (u, v) result from

$$\mathbf{U} = (u, v) = \frac{1}{D+\xi}\int_{-D}^{\xi} \mathbf{V}\, dz, \tag{2}$$

with $\mathbf{D}(\mathbf{x})$ the depth below the undisturbed sea level and $\xi(\mathbf{x}, t)$ the sea-level fluctuations; $\mathbf{V}(\mathbf{x}, t)$ represents the horizontal component of the three-dimensional velocity field.

The relative vorticity ω of a fluid column may be decomposed into

$$\omega = \eta + \Omega \tag{3}$$

for a certain location, where η is called the topographic vorticity induced by stretching and shrinking of the water column being advected over the bottom, and Ω is the vorticity of the tidal wave induced by sea-level variations. We note here that the vorticities ω, Ω and η all refer to depth mean values.

To proceed, we decompose the total velocity $\mathbf{U}$ into $\mathbf{U} = \mathbf{U}_0 + \mathbf{U}_1$, where $\mathbf{U}_0$ is the undisturbed tidal current and $\mathbf{U}_1$ is the topographically induced current. It is assumed that $|\mathbf{U}_1| << |\mathbf{U}_0|$. According to Zimmerman (1980), this requires $|h(\mathbf{x})| << \mathrm{H}$ where $h(\mathbf{x})$ represents topography and H is the mean depth (*see* equation 5 below). The topographic vorticity $\eta = \mathbf{j}.\nabla \times \mathbf{U}_1$, and $\Omega = \mathbf{j}.\nabla \times \mathbf{U}_0$ with $\mathbf{j}$ the unit vector pointing vertically upwards.

By taking the curl of the depth-averaged equations of motion the equation for the topographic vorticity η may be found, as follows:

$$\frac{\partial \eta}{\partial t} + \mathbf{U}_0.\nabla\eta = \frac{(\omega+f)}{\mathrm{H}}\mathbf{U}_0.\nabla h + \frac{r}{\mathrm{H}^2}\mathbf{j}.(\nabla h \times \mathbf{U}_0) - \frac{r\eta}{\mathrm{H}}, \tag{4}$$

in which we have neglected horizontal diffusion.

In equation (4), f = Coriolis parameter and r is the bottom friction coefficient.

The depth $\mathbf{D}(\mathbf{x})$ below the undisturbed sea level is given by

$$\mathbf{D}(\mathbf{x}) = \mathrm{H} + h(\mathbf{x}). \tag{5}$$

Following Zimmerman, bottom friction was parametrized as a linear function of the depth averaged current. Accordingly, r may be estimated to be of the order of

$$r = \mathrm{C}_\mathrm{D}^* \text{ tidal-current amplitude} \tag{6}$$

where C_D, the drag coefficient, is relevant for quadratic friction. Because the tidal-current amplitude is of the order of 1 $\mathrm{m.s^{-1}}$ and $10^{-3} < \mathrm{C_D} < 5\,10^{-3}$ (Heaps, 1978) we find $r \sim 10^{-3}\,\mathrm{m.s^{-1}}$.

Below, we shall study theoretically two separate cases to explain our measurements. In the first case, we shall

neglect the relative vorticity compared to the planetary vorticity f, whereas the second case will treat the full problem.

Case 1: $\omega << f$

Mathematically this is equivalent to neglecting ω compared to f in equation (4). An identical equation was found by Zimmerman (1978) where he studied the residual vorticity, generated by a rectalinear tidal current flowing over the bottom. As explained in the introduction, we prefer to focus on the M_2 tidal vorticity component in this paper. The undisturbed M_2 tidal flow is represented by

$$\mathbf{U}_0=\left[\frac{U_0}{2}\cos(\sigma t-\varphi_u),\ \frac{V_0}{2}\cos(\sigma t-\varphi_v)\right] \tag{7}$$

in which U_0, V_0 represent amplitudes, φ_u, φ_v are phase angles and σ represents the M_2 tidal frequency. The general solution of equation (4) may be written

$$\eta(\mathbf{x}, t)=\sum_{l=0}^{\infty}[\eta_l(\mathbf{x})e^{il\sigma t}+\eta_l^*(\mathbf{x})e^{-il\sigma t}] \tag{8}$$

(*means complex conjugate) which leads to an amplitude equation for $\eta_1(\mathbf{x})$. The exact solution of this equation is possible and will be dealt with later. For the moment, however, we refer to Young (1983) who dealt with this equation in detail applying the moment method. One of his conclusions was that, to solve equation (4), it was allowed to truncate higher harmonics provided that the length scales of the problem are large compared to the tidal displacement. We shall proceed accordingly and neglect the residual current-tidal current interaction and the tidal current harmonic current interaction. This approximation was also used by Huthnance (1973). As a result, the amplitude of the principal (M_2) vorticity component ($l=1$) with frequency σ may be expressed as

$$\eta_1=\frac{1}{r+iH\sigma}\left[f\left(U_0e^{-i\varphi_u}\frac{\partial h}{\partial x}+V_0e^{-i\varphi_v}\frac{\partial h}{\partial y}\right)-\frac{r}{H}\left(U_0e^{-i\varphi_u}\frac{\partial h}{\partial y}-V_0e^{i\varphi_v}\frac{\partial h}{\partial x}\right)\right] \tag{9}$$

In the next section we shall discuss this result in more detail and compare it with our measurements. We now continue with case 2.

Case 2: $\omega=O(f)$

In this case, it is not possible to simplify equation (4) because ω is not small compared to f. Nevertheless, an analytical solution of equation (4) may be found. Before we do so, we note that, in this case, $\omega\approx\eta=O(f)$ because, according to our assumption, Ω remains unchanged and is small compared to the Coriolis parameter f. At any moment in time, the $\mathbf{U}_1$ velocity field by order of magnitude is given by $|\mathbf{U}_1|=O(\eta.1)=O(f.1)$ in which 1 is the length scale over which $\mathbf{U}_1$ varies. Because $|\mathbf{U}_0|\sim 1\ \mathrm{m.s^{-1}}$ and because $f\sim10^{-4}\mathrm{s^{-1}}$, we note that the largest value for 1 is about 1 km because, otherwise, the condition $\mathbf{U}_1<<\mathbf{U}_0$ is violated. According to our observations (*see* below), for such small length scales, the values for $|\eta|$ are between $10^{-5}\mathrm{s^{-1}}$ and $10^{-4}\mathrm{s^{-1}}$, which relaxes the condition for 1 slightly.

We shall be concerned with the problem of a rectilinear M_2 tidal current. Consequently the undisturbed tidal current is represented by

$$\mathbf{U}=(U_0\sin\sigma t,\ 0). \tag{10}$$

Equation (4) may now be written

$$\frac{\partial\eta}{\partial t}+U_0\sin\sigma t\frac{\partial\eta}{\partial x}=\frac{(\eta+f)}{H}U_0\sin\sigma t\frac{\partial h}{\partial x}-\frac{r\eta}{H}-\frac{r}{H^2}U_0\sin\sigma t\frac{\partial h}{\partial y} \tag{11}$$

where we have neglected Ω compared to η. Next, we introduce the variables ψ and $\mathscr{H}$.

$$\psi=\eta e^{-h/H} \tag{12}$$

$$\mathscr{H}=e^{-h/H}. \tag{13}$$

With the help of these variables, we may write equation (11) as

$$\frac{\partial\psi}{\partial t}+U_0\sin\sigma t\frac{\partial\psi}{\partial x}=-fU_0\sin\sigma t\frac{\partial}{\partial x}\mathscr{H}-\frac{r\psi}{H}+\frac{rU_0}{H}\sin\sigma t\frac{\partial}{\partial y}\mathscr{H} \tag{14}$$

Apart from the variables ψ and $\mathscr{H}$, this equation is similar to the equation that Zimmerman (1978) solved and we may proceed accordingly. Introducing

$$\psi=\frac{1}{2\pi}\int_{-\infty}^{\infty}\tilde{\psi}e^{-i\mathbf{k}\cdot\mathbf{x}}d\mathbf{k} \tag{15}$$

$$\mathscr{H}=\frac{1}{2\pi}\int_{-\infty}^{\infty}\tilde{\mathscr{H}}e^{i\mathbf{k}\cdot\mathbf{x}}d\mathbf{k}, \tag{16}$$

we find, for the time variations of $\tilde{\psi}$ at frequency σ denoted $\tilde{\psi}_\sigma$,

$$\tilde{\psi}_\sigma(\mathbf{k}, t)=\tilde{\mathscr{H}}\frac{\gamma}{2}[R^+(b)e^{i\sigma t}-R^-(b)e^{-i\sigma t}] \tag{17}$$

where

$$a=\frac{r}{H_\sigma},\qquad b=k_x\frac{U_0}{\sigma},\qquad \gamma=U_0\left[k_xf-k_y\frac{r}{H}\right],$$

$$R^+(b)=\sum_{\lambda=-\infty}^{\infty}\frac{(a-i\lambda\sigma)}{a^2+(\lambda\sigma)^2}J_{\lambda-1}(b)[J_{\lambda-1}(b)+J_{\lambda+1}(b)]$$

$$R^-(b)=\sum_{\lambda=-\infty}^{\infty}\frac{(a-i\lambda\sigma)}{a^2+(\lambda\sigma)^2}J_{\lambda+1}(b)[J_{\lambda-1}(b)+J_{\lambda+1}(b)]$$

$J_\lambda(b)$ is the Besselfunction of the first kind.

Because of the condition $h<<H$, we have from equations (12) and (13) that $\tilde{\psi}\sim\tilde{\eta}$ and $\tilde{\mathscr{H}}\sim\frac{\tilde{h}}{H}$, where $\tilde{\eta}$ and $\tilde{h}$ represent the Fourier transforms of η and h. As a result, equation (17) may be written as

$$\tilde{\eta}_\sigma(\mathbf{k}, t)\sim\tilde{h}\frac{\gamma}{2H}[R^+(b)e^{i\sigma t}-R^-(b)e^{-i\sigma t}] \qquad (18)$$

where $\tilde{\eta}_\sigma$ denotes the Fourier transform of the topographic vorticity η with frequency σ.

It is interesting to study the solution given by equation (17) as a function of the wave vector $\mathbf{k}=(k_x, k_y)$. For this purpose, the modulus of the ratio $\tilde{\psi}_\sigma/\tilde{\mathscr{H}}$, which may be obtained from equation (17) by dividing by $\tilde{\mathscr{H}}$, is given in Figure 1 for $U_0=0.6$ m.s^{-1} which is a typical value. From this figure, it is clear that the ratio for a certain k_y is largest for $k_x=0$, which means that topographic elements that have a crest parallel to the tide are most effective in vorticity generation. It may be shown that this is the result of differential friction operating over bottom furrows.

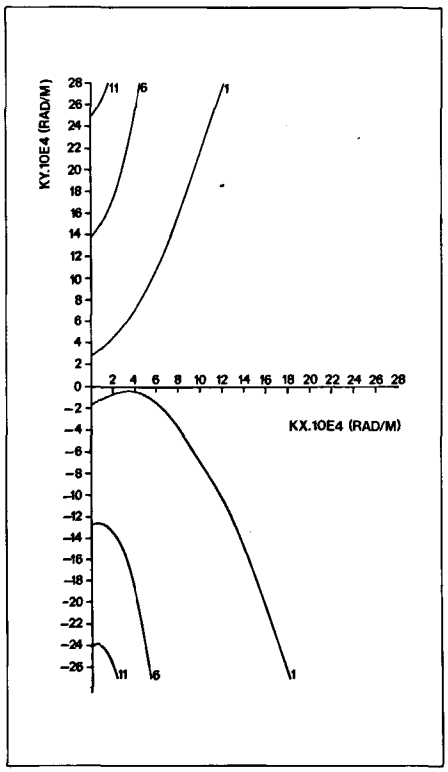

Figure 1
Modulus of the ratio $\tilde{\psi}_\sigma(\mathbf{k})/\tilde{\mathscr{H}}$; *see text below equation* (18).

MEASUREMENTS

In this section, we shall focus on the current measurements. In Figure 2, we have geographically indicated four areas in the Southern Bight of the North Sea in which our current-meter stations were deployed. Within areas 1, 2 and 3, three current-meter stations were installed, while area 4 comprises 14 stations. To reduce wave-induced mooring motions, we have applied a U-shaped mooring with a surface marker and a sub-

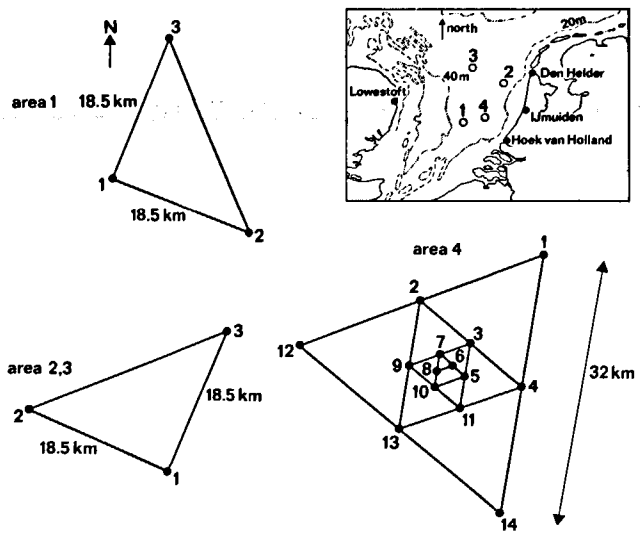

Figure 2
Geographical positions of the areas 1, 2, 3 *and* 4 *where the current measurements were made. The station configuration of area* 4 *is shown schematically.*

surface buoy to provide the necessary buoyancy. At each station, the depth of the current meter was 10 m and the sampling interval was 10 minutes.

In the first 3 areas, the station configuration was a right-angled triangle with sides equal to 10 nautical miles. In the fourth area, the stations were laid out at several separation distances ranging from 2 to 32 km, as indicated schematically in Figure 2. The object of the measurements in area 4 was to study tidal vorticity at different length scales, as will be explained below. Also within areas 2, 3 and 4, self-recording tide gauges were installed to measure tidal sea-level variations. The measuring programme covered the period 1976-1982.

As explained in the introduction, the M_2 tidal constitutent is of major interest in this paper and may be determined by the harmonic tidal analysis method. The M_2 tidal ellipses are shown in Figure 3.

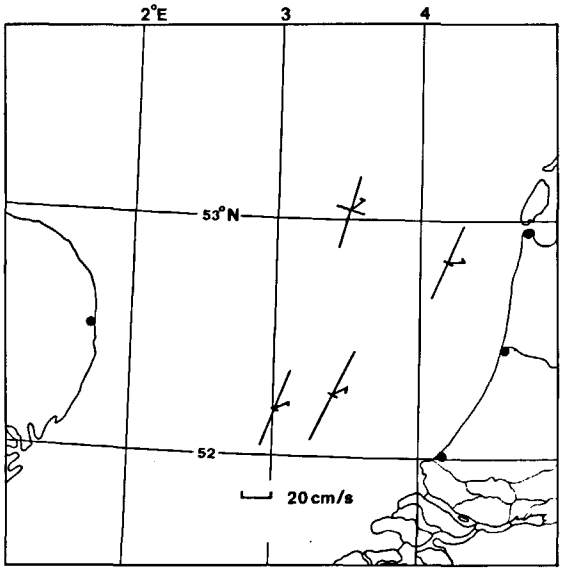

Figure 3
Major and minor axis of the M_2 *tidal ellipse within each area. Sense of rotation of the current (clockwise).*

From Figure 3, we observe nearly rectalinear M_2 tidal currents near the Dutch coast. Area 3 is further offshore near an area where rotating tidal currents are manifest. The M_2 tidal wave within the North Sea was in principle explained by Defant (1925) by considering a reflecting tidal Kelvin wave within a rectangular bay of constant depth (*see* also Krauss, 1973).

We continue with the determination of the M_2 tidal vorticity from our measurements. In this section, vorticity is defined as

$$\bar{\omega}=\frac{\partial V}{\partial x}-\frac{\partial U}{\partial y} \tag{19}$$

where U, V are the Eastern and Northern components of the current measured at 10 m depth. In equation (19) and below, we have used bars to distinguish experimentally deduced vorticities from the theoretically derived vorticities. The M_2 tidal vorticity may be determined with the help of the results of the harmonic tidal analysis. Accordingly, the M_2 contribution to the eastern and northern components of the current may be composed for a tidal cycle. The next step is to calculate $\frac{\partial V}{\partial x}$ and $\frac{\partial U}{\partial y}$ by applying a first-order spatial Taylor expansion. In general, such an operation will result only in an estimated value for the real tidal vorticity, simply because the real vorticity is defined as a (mathematical) point, whereas the estimate is obtained from measurements that are separated by some length L. We shall call the estimated tidal vorticity $\bar{\omega}_L$.

Physical significance of $\bar{\omega}_L$

At one moment during our study, the question was raised about the physical significance of $\bar{\omega}_L$ and it is worthwhile to explore this in more detail. For this purpose, we write the Fourier decompositions of U and V

$$U(\mathbf{x}, t)=\frac{1}{2\pi}\iint_{-\infty}^{\infty}\tilde{U}(\mathbf{k}, t)e^{-i\mathbf{k}\cdot\mathbf{x}}d\mathbf{k} \tag{20}$$

$$V(\mathbf{x}, t)=\frac{1}{2\pi}\iint_{-\infty}^{\infty}\tilde{V}(\mathbf{k}, t)e^{-i\mathbf{k}\cdot\mathbf{x}}d\mathbf{k}. \tag{21}$$

To avoid complex mathematical expressions, we shall consider the situation of a right-angled triangular current-meter array with orthogonal sides equal to L. In this case, $\bar{\omega}_L$, with the help of equations 20 and 21, may be expressed as

$$\bar{\omega}_L(x, t)=\frac{1}{2\pi}\left\{\iint\tilde{V}(k, t)[e^{-i[k_x(x+L)+k_y y]}-e^{-i\mathbf{k}\cdot\mathbf{x}}]\right.$$

$$\left.-\tilde{U}(\mathbf{k}, t)[e^{-i[k_x x+k_y(y+L)]}-e^{-i\mathbf{k}\cdot\mathbf{x}}]d\mathbf{k}\right\}/L \tag{22}$$

After some manipulation, we obtain

$$\bar{\omega}_L(\mathbf{x}, t)=\frac{1}{2\pi}\left[\frac{\partial}{\partial x}\iint_{-\infty}^{\infty}\tilde{V}(\mathbf{k}, t)e^{-i\mathbf{k}\cdot\mathbf{x}}R_x(k_x.L)\,d\mathbf{k}\right.$$

$$\left.-\frac{\partial}{\partial y}\iint_{-\infty}^{\infty}\tilde{U}(\mathbf{k}, t)e^{-i\mathbf{k}\cdot\mathbf{x}}R_y(k_y.L)\,d\mathbf{k}\right] \tag{23}$$

in which

$$R_n(k_n.L)=\frac{e^{-ik_nL}}{-ik_nL}\qquad(n=x, y).$$

The expression given by equation (23) would be equal to the vorticity $\bar{\omega}$ for $R_n=1$. However, $R_n(k_nL)$ turns out to be a low pass filter for wave numbers, as is obvious from Figure 4, where the modulus and phase shift is shown. The cut-off occurs at $L.|\mathbf{k}|=1$. Accordingly, $\bar{\omega}_L(\mathbf{x}.t)$ represents a smoothed vorticity field, from which the variability at spatial length scales smaller than L have been filtered out.

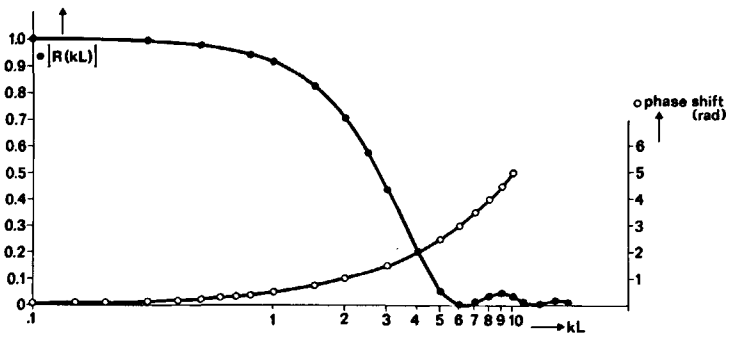

Figure 4
The modulus and phase shift of the low-pass wave-number filter R (KL). ● $|R(kL)|$; ○ *phase shift (rad)*

For later applications, it is also interesting to study the expression $\bar{\omega}_L-\bar{\omega}_{2L}$. With the help of equations (20) and (21), we arrive at

$$\bar{\omega}_L-\bar{\omega}_{2L}=\frac{1}{2\pi}\left[\frac{\partial}{\partial x}\int_{-\infty}^{+\infty}\int_{-\infty}^{+\infty}\tilde{V}(\mathbf{k}, t)e^{-i\mathbf{k}\cdot\mathbf{x}}S_x(k_xL)\,d\mathbf{k}\right.$$

$$\left.-\frac{\partial}{\partial y}\int_{-\infty}^{+\infty}\int_{-\infty}^{+\infty}\tilde{U}(\mathbf{k}, t)e^{-i\mathbf{k}\cdot\mathbf{x}}S_y(k_yL)\,d\mathbf{k}\right] \tag{25}$$

in which

$$S_\eta(k_nL)=\frac{2e^{-ik_nL}-e^{-2ik_nL}-1}{-2ik_nL}\qquad(n=x, y) \tag{26}$$

(derived for a right-angled triangle).

The modulus and phase shift of $S(kL)$ is given in Figure 5, which shows the characteristics of a band-pass filter for wave numbers. The maximum output is for $|\mathbf{k}|.L=2$ with a reduction of 70%. Unfortunately,

the phase response of the filter is not reliable and is better discarded. Obviously, the filter $\bar{\omega}_L - \bar{\omega}_{2L}$ determines approximately the spatial Fourier component of vorticity with a wave length equal to approximately πL.

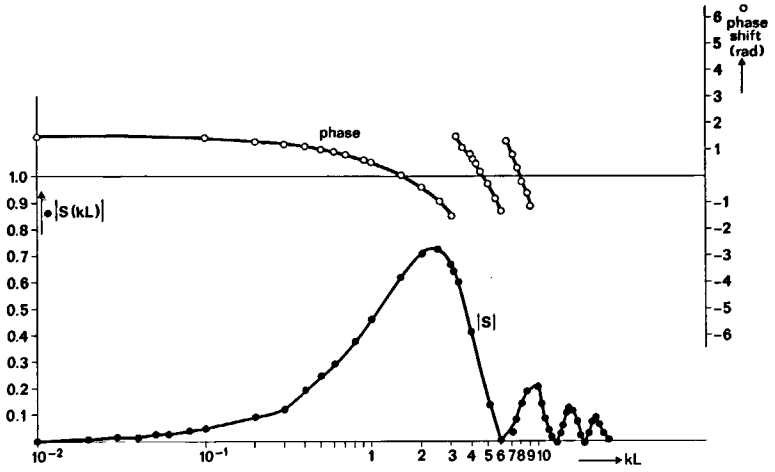

Figure 5
The modulus and phase shift of the band-pass wave-number filter S (kL) that is created by taking $\bar{\omega}_L - \bar{\omega}_{2L}$. ● $|S(kL)|$; ○ *phase shift of S (kL) (rad).*

Determination of topographically induced vorticity

Above we have clarified the nature of our measurements. Next we wish to make a distinction between the vorticity $\bar{\Omega}(t)$ that is generated by the sea-surface variations $\xi(t)$ and the vorticity $\bar{\eta}(t)$ that is generated by the topography $h(\mathbf{x})$ (bars indicate experimentally derived values). Both $\xi(t)$ and $h(\mathbf{x})$ are able to produce vorticity because each may change the length of a water column while it is advected over the bottom during the passage of the tidal wave. In order to make this distinction, we follow Zimmerman (1980) who argued that the depth averaged values for $\bar{\Omega}(\mathbf{x}, t)$ and $\bar{\eta}(t)$ [respectively η and Ω, *see* equation (3)] are additive in first approximation. Here we assume that we may apply the same addition for the vorticity at the 10-m depth level. Based on this assumption, we write

$$\bar{\eta}(\mathbf{x}, t) = \bar{\omega}(\mathbf{x}, t) - \bar{\Omega}(\mathbf{x}, t) \tag{27}$$

where $\bar{\omega}(\mathbf{x}, t)$ is defined by equation (19). We further assume that $\bar{\Omega}(\mathbf{x}, t)$ at the depth of 10 m may accurately be approximated to the depth-averaged value of $\bar{\Omega}(\mathbf{x}, t)$, denoted $\Omega(\mathbf{x}, t)$, which according to Zimmerman (1978) is equal to

$$\bar{\Omega}(\mathbf{x}, t) \sim \xi(\mathbf{x}, t)\frac{f}{H}. \tag{28}$$

In order to apply equation (27) to our experimental data, we write

$$\bar{\eta}_L(\mathbf{x}, t) = \bar{\omega}_L(\mathbf{x}, t) - \bar{\Omega}(\mathbf{x}, t) \tag{29}$$

where $\bar{\eta}_L$ and $\bar{\omega}_L$ represent the smoothed vorticity fields as explained above. To arrive at equation (29), the assumption was made that $\bar{\eta}(\mathbf{x}, t)$ and $\bar{\Omega}(\mathbf{x}, t)$ vary over different horizontal length scales.

According to this assumption, $\bar{\eta}(\mathbf{x}, t)$ is organized on length scales imposed by the bottom topography which seems a logical consequence of the fact that $\bar{\eta}(\mathbf{x}, t)$ represents the topographic vorticity. However, as argued by Zimmerman, the variability of the tidal sea-level variations $\xi(\mathbf{x}, t)$ is organized on larger length scales, and according to equation (28) the same holds for $\bar{\Omega}(\mathbf{x}, t)$. Implicit in this reasoning is the assumption that bottom topography mainly modifies the currents while the sea surface remains relatively undisturbed.
With the help of our tide gauge data and equation (28), we found that, by order of magnitude, the amplitude of $\bar{\Omega}(\mathbf{x}, t)$ is equal to about 1/3 of the amplitude of $\bar{\omega}_L(\mathbf{x}, t)$, for $L = 10$ nautical miles. We may conclude therefore that most of the vorticity that we have measured is topographically induced. Of course, this may be partly explained by considering the bottom topographic elements which may have large amplitudes compared to the tidal sea-level variations $\xi(t)$. The amplitudes of the latter are between 0.5 and 1 m for the M_2 tide, whereas the water depth may show variations up to several metres. Accordingly, the length of a water column may for the greater part, be changed by topography. As we have shown above, this only partly explains $\bar{\omega}_L(t)$ because bottom friction may be of equal importance or even dominate for length scales small compared to the tidal displacement.

Presentation of topographically induced vorticity

First, we shall present the M_2 topographically induced vorticities that we have measured in areas 1, 2 and 3. In Figure 6 the M_2 topography vorticity time series, determined after a harmonic analysis of the tidal measurements, is shown for a tidal cycle. It may be observed that the M_2 vorticity amplitudes are of the order of $5.10^{-6}\,s^{-1}$. Similar curves (not shown) were also prepared for the M_4 tidal vorticity component. From these curves, we found that the amplitudes of the M_4 vorticity were typically of the order of $5.10^{-7}\,s^{-1}$.
At this point it is important to consider the measurement errors. For this reason, we note that, by factory specification, the accuracy of the current-metres is $\Delta U \sim 1\ cm.s^{-1}$. However, this is only one source of error. Another source is related to the accuracy with which the tidal current constituents may be determined in case of a relatively short record length. We believe we have minimized such errors, because the currents were measured simultaneously, and consequently the large-scale tidal wave was the same for all stations within a certain area. To have an indication for the errors, we determined the difference between the original current-meter time series and the tidal harmonic series. Typically, the standard deviation of this difference is $5\ cm.s^{-1}$. Combining these error estimates, the total error ΔU is about $6\ cm.s^{-1}$. For $L = 10$ nautical miles, the vorticity error may be estimated to be $\Delta U/L \sim 3.10^{-6}\,s^{-1}$ approximately. Relative to the M_4 vorticity amplitudes ($\sim 5.10^{-7}\,s^{-1}$), these errors are unacceptably high and these data should be discarded. The M_2 data may be considered physically significant, although the errors are certainly not small. The above-

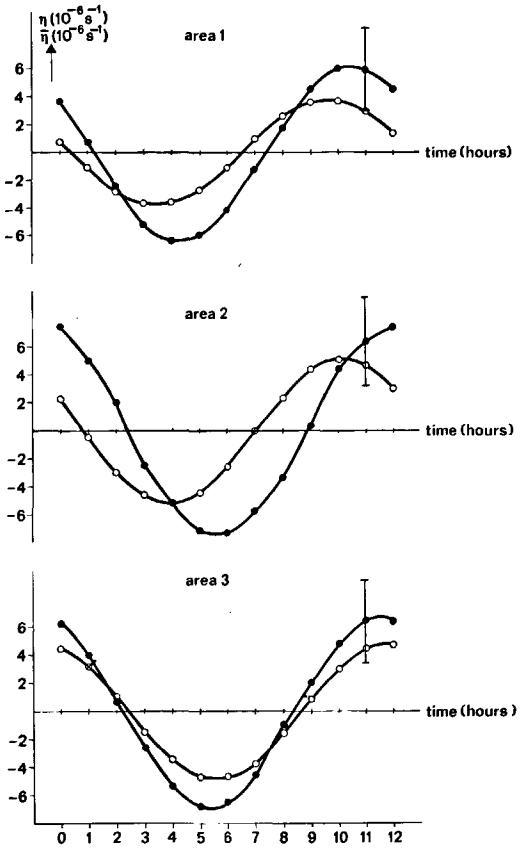

Figure 6
M_2 topographic time series for areas 1, 2 and 3. ● measured topographic vorticity: $\bar{\eta}(t)$; ○ theoretically predicted topographic vorticity: $\eta(t)$. Error bars for the measurements are indicated

mentioned errors should be regarded as maximum values, because the non-vanishing difference of the harmonic tidal analyses is also contaminated with non-tidal contributions, such as wind-driven currents which are variable in time.

The next set of topographic vorticity values that we shall present refer to the data of area 4. The purpose of the measurements in this area was to be able to study vorticity as a function of length scale. To do this, we shall make use of the bandpass filter described by equation (25) which, because of equation (29), is equally valid for $\bar{\eta}_L - \bar{\eta}_{2L}$.

In Figure 7 we have depicted the experimentally determined Fourier transform of the M_2 topographic vorticity amplitudes $\bar{\eta}_L$ as a function of the length scale L, from which we observe increasing vorticity amplitudes for decreasing length scales up to the smallest separation distance that we have used.

COMPARISON AND DISCUSSION

This section will deal with the comparison of our experimental data with the theory and a discussion of the results. Of first concern will be the data obtained in areas 1, 2 and 3 for which equation (9) will be the starting point. The interest is in large length scales. To evaluate equation (9), it is important to have available accurate information about the bottom topography.

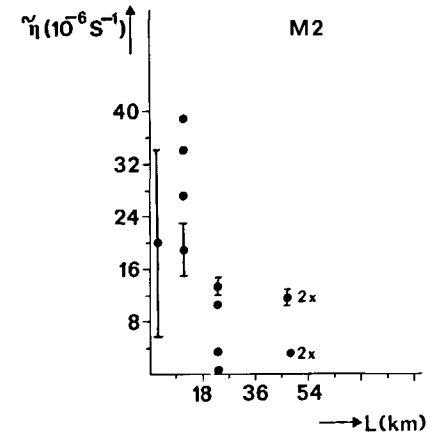

Figure 7
M_2 topographic vorticity amplitudes as a function of the length scale L based upon the measurements in area 4. Error bars are included (2x: means coinciding points).

Unfortunately, this presents a serious problem even in a well known sea area like the Southern Bight. Some information may be obtained from the depth measurements that were performed when the current-metre stations were deployed. However, these are point measurements and may not be representative of the area around the station. On the other hand, depth surveys were conducted in the past to construct navigational charts. These measurements are very accurate and are performed on a very small scale (± 250 m). In practice, the bottom topography of an area with a size of 10×10 nautical miles may be obtained from a composite of different depth surveys. Because priorities are not restricted to one area, the depth composites are based on surveys conducted over a period of several years. Unfortunately, during such a period, the bottom topography may have been subject to modifications caused by surface waves or currents manifest over the area. Indeed, from such surveys, we found depth differences for partly overlapping tracks, although the larger-scale features were found to be similar. Nevertheless, the data of these depth surveys are the most accurate known to date for the Southern Bight. In order to proceed, we shall assume that the large-scale bottom topography is reasonably stable. According to this assumption, we were able to construct Table 1 which shows $\nabla h(\mathbf{x})$ for areas 1, 2 and 3. The depth data around each current-metre station were averaged to obtain these gradients.

Table 1
Bottom topographic gradients.

Area	$\frac{\partial h}{\partial x}$	$\frac{\partial h}{\partial y}$	H (*m*)
1	$-2.7.10^{-4}$	$2.7.10^{-4}$	32
2	$-1.1.10^{-4}$	$-1.6.10^{-4}$	24
3	$-3.2.10^{-4}$	$-3.2.10^{-4}$	27

By order of magnitude, it may be observed from Table 1 that $|\nabla h| \sim 10^{-4}$ which means that, on average, the depth may change several metres within our areas 1, 2 and 3.

Next in the evaluation of equation (23), we need to know the undisturbed tidal current $U(t)$ which would be flowing if there was no bottom topographical feature to guide it locally. Of course, this should be done theoretically in a zero-order approximation of the problem in which topography is absent. Instead, however, we realize that the topographic flow disturbances are small. For L = 10 nautical miles, they may be estimated, with the help of our vorticity measurements, to be $\bar{\omega}_L{}^* L \sim 10$ cm.s^{-1} at most. Accordingly, a reasonable estimate for U may be obtained from the mean M_2 tidal-current component within each area.

Finally, the theoretically predicted topographic M_2 tidal vorticity time series is shown in Figure 6, together with the observed ones. A good agreement may be observed although minor discrepancies are manifest. We attribute these discrepancies mainly to topographic inaccuracies. On the other hand, the information on the bottom friction coefficient r may not be accurate. Small variations of r within physical limits did not improve our results, however.

We continue with the discussion of the vorticity measurements conducted in area 4. It was noted already that our measurements agree, in principle, with our theoretical deductions since we found that the vorticity amplitudes increase for decreasing length scales. The response function given in Figure 1 predicts this behaviour precisely. It would be of interest, however, to make a more precise comparison, with the help of the actual bottom topography. In principle, this is possible because precise depth measurements are available, as described above. Unfortunately, we have no information on the stability, especially of the smallest scale topographic elements which are of major interest for area 4. We found, on the contrary, some evidence that small-scale modifications have taken place. For this reason, we have not tried to compare our small-scale measurements in great detail with the theoretically predicted vorticity values. Nevertheless, it is worthwhile exploring the bottom topography of area 4. For this reason, we prepared Figure 8 which shows the depth distribution of area 4 on a 500-m grid. The unfiltered FFT transform of this distribution is given in Figure 9. From this figure, it is noteworthy that the variability of the bottom topography is restricted mainly into the k_y-direction. The response function given in Figure 1 attains its largest values precisely in this direction. A rough comparison may be performed between our measurements and the results of the theoretical section. For this purpose, we note that the Fourier transform of the amplitude of the M_2 topographic vorticity, $\bar{\eta}_\sigma(\mathbf{k}, t)$, is given by equation (18). We shall evaluate equation 18 for $k_x = 0$. In order to do this, the bottom topographic spectrum shown in Figure 9 was filtered first by averaging 5 wave number bands along the k_y-axis. In this way, 3 topographic amplitudes $\tilde{h}(k_y)$ were found centered around $k_y = 2.1.10^{-3}$, 4.10^{-3} and $5.6.10^{-3}$ rad.m^{-1} corresponding to the length scales L = 3, 1.6 and 1.1 km. With the help of equation (18), we arrive at the data shown in Table 2 where, for the four length scales of concern, the amplitude $\bar{\eta}_\sigma(\mathbf{k})$ is shown. The results shown in Table 2 may be compared

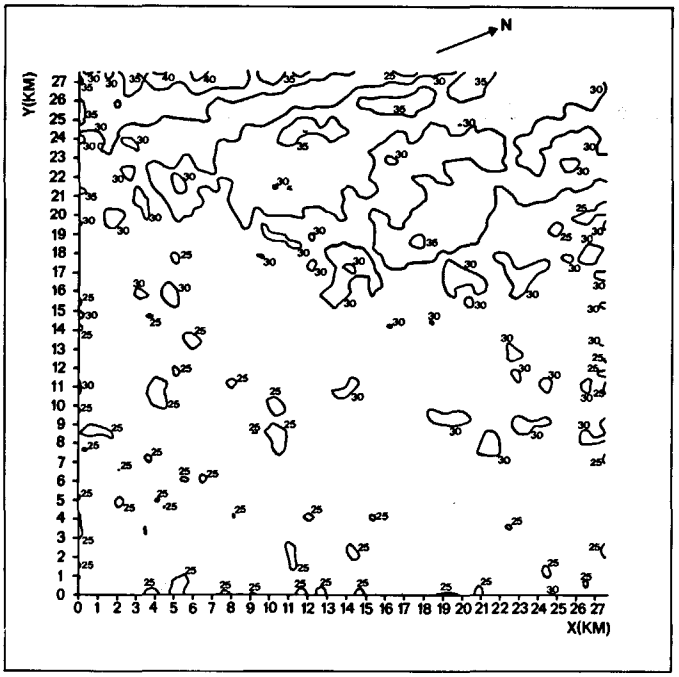

Figure 8

Bottom topography of area 4. Depth isolines are shown every 5 m. The x-axis is parallel to the major axis of the tidal current.

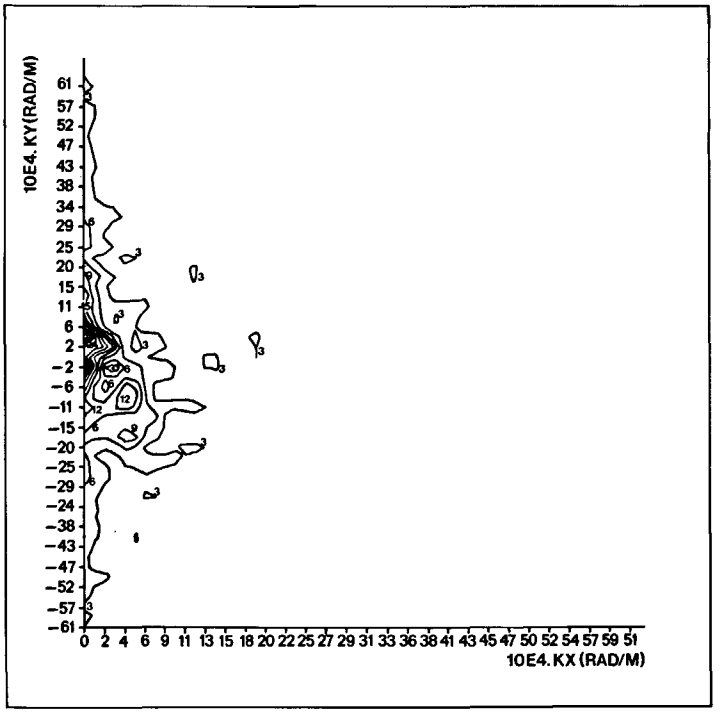

Figure 9

The two-dimensional spectrum of the bottom topography, $\tilde{h}(\mathbf{k})$, of the depth shown in Figure 8. Shown in this figure is the unfiltered spectrum that was calculated with the help of a FFT algorithm $\mathbf{k} = (k_x, k_y)$.

Table 2

Theoretically predicted M_2 vorticity amplitude as a function of the length scale L for $k_x = 0$.

k_y (rad/m)	L (km)	$\tilde{\eta}_\sigma(k_y)$ (s^{-1})
21.10^{-4}	3	$2.1.10^{-4}$
40.10^{-4}	1.6	$2.3.10^{-4}$
56.10^{-4}	1.1	$2.3.10^{-4}$

with the data depicted in Figure 7. As is obvious from an inspection of Figure 7 and Table 2, the measurements indicate smaller vorticity amplitudes, where the ratio is approximately one order of magnitude. Although it is to be remembered that the topography shown in Figure 8 may not be very accurate as to the precise location, especially of the small-scale bottom topographic elements, we may assume that the order of magnitude of the heights of these elements may very well be estimated with the help of this topography. Reduction of the friction coefficient r would result in lower theoretically predicted vorticity amplitudes. Indeed the arguments of Heaps (1978) may give rise to $r=2.10^{-3}\,\mathrm{m.s^{-1}}$ compared to the value of $r=5.10^{-3}\,\mathrm{m.s^{-1}}$ that we have used. However, Heaps' value does not explain the difference of one order of magnitude that we have found. An explanation of the differences that we have found above at present cannot be given. However, because, in our situation, bottom friction is the prime candidate for small-scale vorticity generation, we suspect that the simple linear friction law is not adequate and needs modification. Indeed, it is well known from turbulence theory that a quadratic friction law is more appropriate.

CONCLUSIONS

It was shown experimentally that, within an apparently homogeneous shallow sea area, significant tidal-current differences may be manifest over relatively short horizontal distances. For the M_2 tidal component of the current, these differences may not be attributed entirely to measurement errors. A convenient way to quantify these current differences are vorticity values which make them accessible for theoretical explanation.

In this way, the M_2 tidal vorticity could be explained by considering the interaction of the M_2 tidal current with the bottom topography. For large length scales, a quantitative comparison between theory and experiment yielded good results. For length scales small compared to the tidal displacement, a qualitative comparison was carried out, because the small-scale bottom topography is not well known. From this rough comparison, we found strong indications that a linear bottom friction law is not adequate to describe the interaction of the tidal current with bottom topography.

For engineering purposes, it is perhaps useful to know that we observed that the vorticity amplitude is of the order of $5.10^{-6}\,\mathrm{s^{-1}}$, which implies that the velocity may vary up to $10\,\mathrm{cm.s^{-1}}$ within an area of 10×10 nautical miles. Of course, this is only valid for the areas of our research.

Acknowledgements

The author wishes to thank L. Otto and G. J. Komen of KNMI for critically reading the original version of the manuscript and for the subsequent stimulating discussions.

REFERENCES

Butman B., Noble M., 1983. An upper bound for the tidally rectified current at one location on the southern flank of Georges Bank, *J. Phys. Oceanogr.*, **13**, 1452-1460.

Defant A., 1925. Gezeitenprobleme aus Meeres in Landnähe, in: *Probleme der Kosmischen Physik, vol. VI,* Henry Grand Hamburg.

Heaps N. S., 1978. Linearized vertically integrated equations for residual circulation in coastal seas, *Dtsch. Hydrogr. Z.*, **31**, 5, 147-169.

Huthnance J. M., 1973. Tidal current assymmetries over the Norfolk Sandbanks, *Estuarine Coastal Mar. Sci.*, **1**, 89-99.

Komen G. J., Riepma H. W., 1981*a*. The generation of residual vorticity by the combined action of wind and bottom topography in a shallow sea, *Oceanol. Acta*, **4**, 3, 267-277.

Komen G. J., Riepma H. W., 1981*b*. Residual vorticity induced by the action of tidal currents in combination with bottom topography in the Southern Bight of the North Sea, *Geophys. Astrophys. Fluid Dyn.*, **18**, 93-110.

Krauss W., 1973. *Methods and results of theoretical oceanography, part* 1, Gebrüder Borntraeger, Berlin, 302.

Loder J. W., 1980. Topographic rectification of tidal currents on the sides of Georges Bank, *J. Phys. Oceanogr.*, **10**, 1399-1416.

Magnell B. A., Spiegel S. L., Scarlet R. I., Andrews J. B., 1980. The relationship of tidal and low frequency currents on the north slope of Georges Bank, *J. Phys. Oceanogr.*, **10**, 1200-1212.

Riepma H. W., 1980. Residual currents in the North Sea during in/out of Jonsdap 76, *Meteor Forschungsergebn., Reihe A*, **22**, 19-32.

Riepma H. W., 1985. Current meter records and the problem of the simulation of particle motions in the Southern Bight of the North Sea near the Dutch coast, *Oceanol. Acta*, **8**, 4, 403-412.

Riepma H. W., 1986. Note on observed vorticity of residual currents in an area of the Southern Bight of the North Sea, *Dtsch. Hydrogr. Z.*, **39**, 4, 161-167.

Robinson I. S., 1981. Tidal vorticity and residual circulation, *Deep-Sea Res.*, **28A**, 3, 195-212.

Tee K. T., 1977. Tide induced residual current. Verification of a numerical model, *J. Phys. Oceanogr.*, **7**, 396-402.

Yanagi T., 1976. Fundamental study of the tidal residual circulation, *J. Oceanogr. Soc. Jpn*, **32**, 199-208.

Yasuda H., 1980. Generating mechanism of the tidal residual current due to the coastal boundary layer, *J. Oceanogr. Soc. Jpn*, **35**, 241-252.

Young W. R., 1983. Topographic rectification of tidal currents, *J. Phys. Oceanogr.*, **13**, 716-721.

Zimmerman J. T. F., 1978. Topographic generation of residual circulation by oscillatory tidal currents, *Geophys. Astrophys. Fluid Dyn.*, **11**, 35-47.

Zimmerman J. T. F., 1980. Vorticity transfer by tidal currents, *J. Mar. Res.*, **38**, 4, 601-630.